RESEARCH ARTICLE

Degradation of 1,2-dichloroethane by photocatalysis using immobilized PAni-TiO$_2$ nano-photocatalyst

Mahdi Mohsenzadeh[1] · Seyed Ahmad Mirbagheri[2] · Samad Sabbaghi[3]

Abstract

1,2-Dichloroethane is one of the most hazardous environmental pollutants in wastewaters. It is mainly used to produce vinyl chloride monomer, the major precursor for PVC production. It is determined to be a probable human carcinogen and has been listed as a priority pollutant by the United States Environmental Protection Agency. Due to high chemical stability and low biodegradability of 1,2-dichloroethane, heterogeneous photocatalysis was used for degradation of this chlorinated hydrocarbon. PAni-TiO$_2$ nanocomposite was synthesized by in situ deposition oxidative polymerization method and immobilized on glass beads by a modified dip coating and heat attachment method. The characteristics of synthesized PAni-TiO$_2$ nanoparticles were confirmed using the results of morphology tests including Fourier-transform infrared spectra, X-ray diffraction patterns, particle size analysis, UV-Visible spectrophotometer, scanning electron microscope, and energy-dispersive X-ray spectroscopy. The performance of photocatalytic degradation of 1,2-dichloroethane using synthesized PAni-TiO$_2$ nanocomposite in a designed and constructed pilot scale packed bed recirculating photocatalytic reactor under xenon light irradiation was investigated. The response surface methodology based on the central composite design was used to evaluate and optimize the effect of 1,2-dichloroethane concentration, residence time, pH, and coating mass as independent variables on the photocatalytic degradation of 1,2-dichloroethane as the response function. Results showed that actual and predicted results were well fitted with R^2 of 0.9870, adjusted R^2 of 0.9718, and predicted R^2 of 0.9422. The optimum conditions for 1,2-dichloroethane photocatalytic degradation were the 1,2-dichloroethane concentration of 250 mg/L, the residence time of 240 min, pH of 5, and coating mass of 0.5 mg/cm^2, which resulted in 88.84% photocatalytic degradation. Kinetic of the photocatalytic degradation at optimal condition follows the Langmuir-Hinshelwood first-order reaction with $k = 0.0095$ min^{-1} with $R^2 = 0.9455$. Complete photocatalytic degradation of 1,2-DCE was achieved after 360 min.

Keywords PAni-TiO$_2$ · 1,2-Dichloroethane · Photocatalytic degradation · Pilot-scale photoreactor · Response surface methodology · Immobilization

---

✉ Samad Sabbaghi
   sabbaghi@shirazu.ac.ir; samad.sabbaghi@uwaterloo.ca

   Mahdi Mohsenzadeh
   mohsenzadeh@mail.kntu.ac.ir

   Seyed Ahmad Mirbagheri
   mirbagheri@kntu.ac.ir

[1] Department of Environmental Engineering, Faculty of Civil Engineering, K.N. Toosi University of Technology, Tehran, Iran

[2] Department of Environmental Engineering, Faculty of Civil Engineering, K.N. Toosi University of Technology, Tehran, Iran

[3] Nanochemical Engineering Department, Faculty of Advanced Technologies, Shiraz University, Shiraz, Iran

Introduction

Chlorinated hydrocarbons are among the pollutants that are frequently detected in industrial wastewaters (Vazirzadeh et al. 2012). 1,2-Dichloroethane (1,2-DCE) is one of the most important chlorinated hydrocarbons that is not found naturally in the environment. It is mainly used in the petrochemical industry for the production of vinyl chloride, the main precursor for PVC production (Huang et al. 2014). Public exposure to 1,2-DCE can occur from breathing contaminated air or consumption of contaminated water. Breathing in 1,2-DCE can cause irritation to the eyes, skin, nose, throat, and lungs. Ingestion can cause effects on the liver, kidneys, and nervous system (Tian et al. 2019; Wang et al. 2016; Wang et al. 2017). It is determined to be a probable human carcinogen and has been

listed as a priority pollutant by the United States Environmental Protection Agency (U.S. EPA) (Pham et al. 2009). The maximum contaminant level (MCL) for 1,2-DCE in drinking water is 5 μg/L and the maximum contaminant level goal (MCLG) is set as zero by the U.S. EPA (Liu et al. 2014).

Iran is one of the largest polyvinyl chloride (PVC) producers in the world. Arvand petrochemical complex, located at Bandar Imam, was founded in 2010. In 2012, about 300,000 tons of polyvinyl chloride (PVC) was produced at the Arvand petrochemical complex. Bandar Imam Khomeini, Abadan, and Qadir are the three other petrochemical complexes producing PVC with an aggregate production capacity of over 405,000 tons per year (Bijhanmanesh and Etesami 2016; Maleki et al. 2016). During the production of 1000 kg of 1,2-DCE, about 0.4 m^3 wastewater with 50–200 mg/L of 1,2-DCE is produced (Eydivand and Nikazar 2015). It is obvious that 1,2-DCE is a major environmental pollution in Iran's petrochemical industry. Therefore, this synthetic compound was selected as the target pollutant in the present study.

Physical, chemical, and biological treatment processes have been studied for 1,2-DCE degradation (Bejankiwar et al. 2005; De Wildeman et al. 2001; Eydivand and Nikazar 2015; Lin et al. 2014; Liu et al. 2014; Mohsenzadeh et al. 2019a; Pham et al. 2009). 1,2-DCE is a low biodegradable and chemically stable environmental pollutant. Therefore, heterogeneous photocatalysis was selected as a non-selective process for degradation of 1,2-DCE by oxidation through reactions with reactive species (hydroxyl radicals and super oxide radicals) (Hajian et al. 2017; Hung et al. 2008).

TiO_2 is widely used as a photocatalyst. However, the low overlap between the absorption spectrum of TiO_2 and the visible spectrum decrease the photoreaction rates. In addition, the photocatalytic activity is decreased by the recombination of electron-hole pairs (Mohammadi and Sabbaghi 2014). The composition of polyaniline (PAni) and TiO_2 results in reducing band gap energy and hindering recombination (Hung et al. 2017; Radoičić et al. 2017; Sabbaghi et al. 2015; Salem et al. 2009; Yang et al. 2017). PAni-TiO_2 nanocomposite was synthesized in previous studies by different methods including sol-gel technique (Schnitzler and Zarbin 2004), hydrothermal method (Lin et al. 2012), and in situ deposition oxidative polymerization method (Zhang et al. 2006). PAni-TIO_2 nanocomposite was immobilized on some supports previously (Hung et al. 2008; Jinzhang et al. 2007).

Response surface methodology (RSM) is a set of mathematical relationships and statistical techniques for seeking the optimum response parameter of complicated multivariable processes with the lowest number of tests. RSM has been successfully applied to photocatalytic degradation of pollutants (Antonopoulou et al. 2017; Mohsenzadeh et al. 2019b; Nam et al. 2018; Nekouei and Nekouei 2017).

In this study, a new pilot scale packed bed recirculating batch photocatalytic reactor was designed and constructed for photocatalytic degradation experiments. The reactor specifications are reported in the present study. In addition, PAni-TiO_2 nanocomposite was synthesized and immobilized on glass beads by a modified dip coating and heat attachment method. The characteristics of nanoparticles were confirmed using FTIR, XRD, PSA, UV-Vis spectroscopy, SEM, and EDS techniques. The response surface methodology (RSM) based on central composite design (CCD) was used for modeling and optimization of the effect of 1,2-DCE concentration, residence time, pH, and coating mass as independent parameters on the photocatalytic degradation of 1,2-DCE as the response parameter. Also, kinetic of the photocatalytic degradation at optimal condition was studied.

Experimental

Chemicals and materials

All chemicals used were of analytical reagent grade and were used as received. 1,2-Dichloroethane, aniline, n-hexane, hydrochloric acid fuming 37%, hydrofluoric acid, sodium hydroxide, and ethanol were obtained from Merck (Germany). Diethyl ether was obtained from Riedel-de Haën (Germany). Ammonium peroxydisulfate (APS) ($(NH_4)_2S_2O_8$) was obtained from Fluka. TiO_2 nanopowder (anatase phase with average crystal size of 20 nm) was obtained from US Nano. Deionized water was used for solution preparation throughout this research.

Analytical method

Sample collection and preservation was carried out according to standard methods 6010 B. At specified sampling times, 35 mL of the wastewater was added to a 40-mL glass vial containing 2 mL of n-hexane. Vigorous mixing using Vortex mixer at 3200 rpm for 2 min extracted all relevant organic compounds. The extraction vials were turned upside down to avoid loss to the headspace and placed into a refrigerator at 4 °C. After that, 1 mL was withdrawn from the hexane phase of the extraction vial and transferred into a 2-mL autosampler vial for analysis. Autosampler vials were sealed with parafilm and were stored in − 80 °C laboratory freezer prior to analysis (APHA 2012).

Samples were analyzed based on standard methods 6200 B. A DB-5 capillary column with an inner diameter of 0.32 mm and a film thickness of 1.5 μm was used. The autosampler vials were automatically inserted into the GC injection port. The oven temperature was increased to 35 °C and was kept at this temperature for 2 min. Subsequently, the oven temperature rose to 200 °C with a ramp of 10 °C/min and

kept at this temperature for 5 min. Afterward, the oven temperature was increased to 225 °C with a ramp of 20 °C/min and kept at this temperature for 1 min (APHA 2012). Gas chromatography analysis was carried out using a gas chromatograph (Agilent technologies 7890 B GC system) with mass selective detector (7955 A MSD).

Synthesis of PAni-TiO$_2$

The PAni-TiO$_2$ nanocomposite was synthesized by in situ deposition oxidative polymerization method. As shown in Figs. 1 and 2.4 g of TiO$_2$ nanopowder and 1 mL aniline were dispersed in 90 mL of 1 M HCl 37% solution under ultrasonic vibration and mixed by a magnetic stirrer for 1 h in an ice water bath in the presence of nitrogen gas. Next, 2.5 g APS was dissolved in 100 mL of 1 M HCl solution and added to the initial TiO$_2$-aniline solution during 1 h. The obtained solution was allowed to be polymerized for 4 h. Later, the resulting precipitated PAni-TiO$_2$ (Fig. 2a, c) was filtered and washed with deionized water, ethanol, and ether. After the filtered material was dried in an oven for 8 h at 80 °C, PAni-TiO$_2$ nanocomposite powder was obtained (Sabbaghi et al. 2015; Zhang et al. 2006).

Immobilization of PAni-TiO$_2$

Immobilization of PAni-TiO$_2$ nanocomposite on glass beads was carried out by a modified dip coating and heat attachment method (Balasubramanian et al. 2003; Khalilian et al. 2015; Khataee 2009; Sakthivel et al. 2002; Salma et al. 2016). As shown in Fig. 3, glass beads with 10 mm diameter were etched with hydrofluoric acid 5% for 24 h and were washed with deionized water for making a rough surface on glass beads. The slurry solution (2.4 g of PAni-TiO$_2$ nanocomposite powder in 200 mL deionized water) was prepared and

continuously mixed for 24 h. The uncoated glass beads were counted and weighted precisely and put in the stainless steel mesh which was immersed in the slurry. The glass beads were mixed for 30 min by a magnetic stirrer (Fig. 2b) and then removed from the suspension and placed in an oven for 30 min at 80 °C to dry (Fig. 2d), and afterward, the glass beads were heat-treated by using a programmable furnace. The furnace temperature increased to 100 °C with a ramp of 3 °C/min and kept at 100 ° C for 1 h. Next, the temperature increased to 550 °C with a ramp of 3 °C/min and was kept at this temperature for an hour. Thereupon, the furnace was allowed to cool down naturally. This heat attachment method causes partial sintering of the particles and adhesion of PAni-TiO$_2$ particles to the glass beads without the need for binders. Ultimately, the unattached photocatalyst particles were washed with deionized water and the beads were dried and weighted again. Coating mass was obtained as follows:

$$\text{Coating mass} = \frac{W}{nA} \qquad (1)$$

where W is the difference between the weight of uncoated and coated glass beads, n is the number of coated glass beads, and $A = 4\pi r^2$ is the surface area of one glass bead with radius r. Coating process was repeated several times until certain coating mass (i.e.: 0.4, 0.5, 0.6, 0.7, and 0.8 mg/cm^2) was reached.

Characterization of PAni-TiO$_2$ Nanocomposite

(PAni:TiO$_2$) with different catalyst compositions, i.e. ((1:0.3), (1:1), (1:1.7), (1:2.4), and (1:3.1)), were synthesized previously. These compositions were determined based on literature and preliminary experiments. Based on the photocatalytic degradation experiments, PAni:TiO$_2$ with (1:2.4) composition was found as the optimal composition for 1,2-DCE
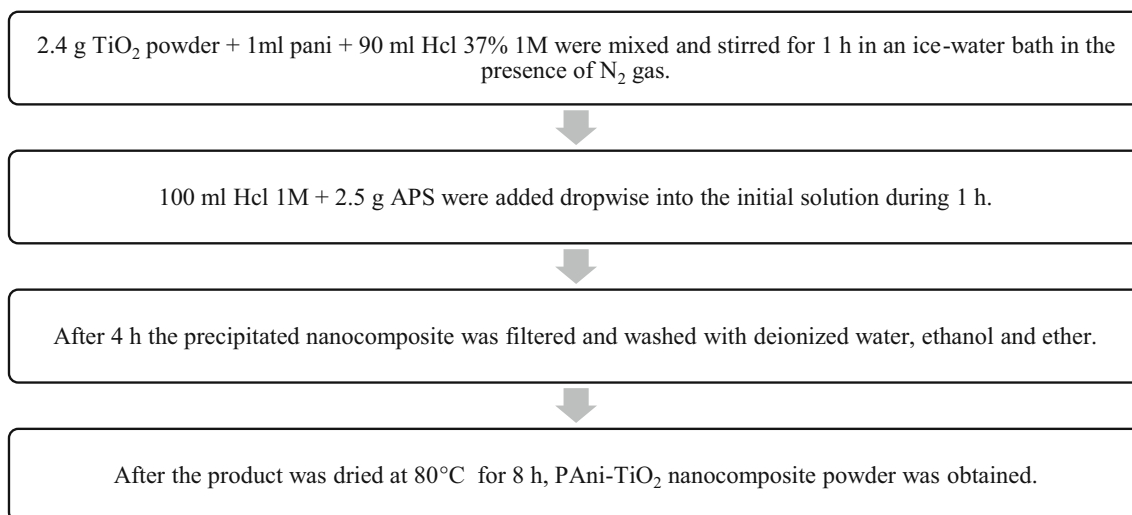
2.4 g TiO$_2$ powder + 1ml pani + 90 ml Hcl 37% 1M were mixed and stirred for 1 h in an ice-water bath in the presence of N$_2$ gas.

↓

100 ml Hcl 1M + 2.5 g APS were added dropwise into the initial solution during 1 h.

↓

After 4 h the precipitated nanocomposite was filtered and washed with deionized water, ethanol and ether.

↓

After the product was dried at 80°C for 8 h, PAni-TiO$_2$ nanocomposite powder was obtained.

Fig. 1 Flowchart of synthesis of PAni-TiO$_2$ nanocomposite

Fig. 2 Images of **a** and **c** synthesis and **b** and **d** immobilization of PAni-TiO$_2$ on glass beads
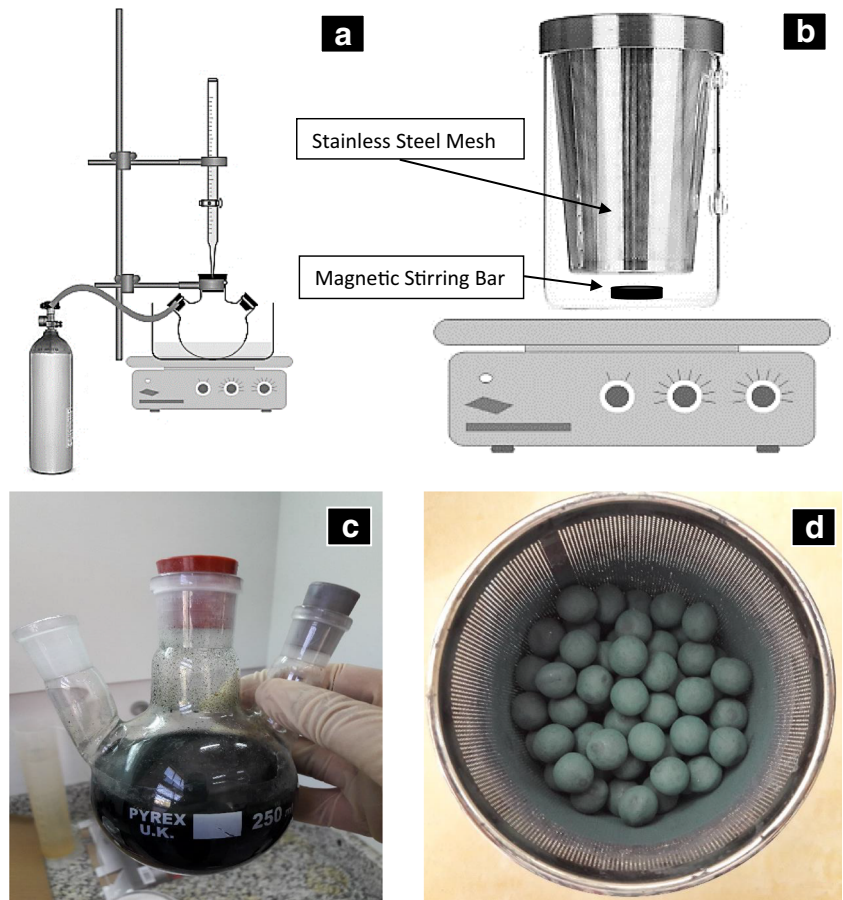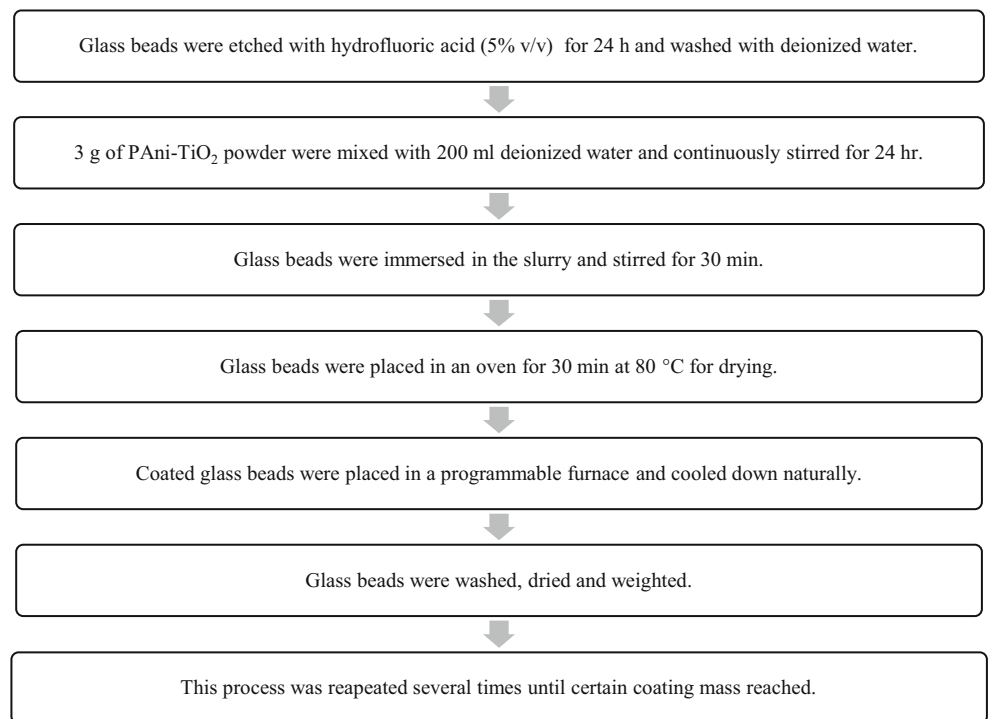

Fig. 3 Flowchart of PAni-TiO$_2$ immobilization on glass beads

Glass beads were etched with hydrofluoric acid (5% v/v) for 24 h and washed with deionized water.

3 g of PAni-TiO$_2$ powder were mixed with 200 ml deionized water and continuously stirred for 24 hr.

Glass beads were immersed in the slurry and stirred for 30 min.

Glass beads were placed in an oven for 30 min at 80 °C for drying.

Coated glass beads were placed in a programmable furnace and cooled down naturally.

Glass beads were washed, dried and weighted.

This process was reapeated several times until certain coating mass reached.

degradation (Mohsenzadeh et al. 2019a). In this study, PAni:TiO$_2$ with (1:2.4) composition was synthesized, characterized, and used for photocatalytic degradation of 1,2-DCE. Different tests including the FTIR, XRD, PSA, UV-spectroscopy, SEM, and EDS were used for characterization of synthesized PAni-TiO$_2$ nanocomposite. The Fourier-transform infrared spectra were recorded with FTIR spectrometer (spectrum RXI, PerkinElmer). X-ray diffraction patterns (XRD) were recorded using a scattering detector Bruker D8 Advance (Billerica, MA) at a voltage of 40 kV and 45 mA using radiation CuKα ($\lambda = 1.5406$ Å). The XRD pattern data were collected for the 2θ values between 10 and 90° and a scanning rate of 0.02°/s. Particle size analysis (PSA) test was performed using HORIBA DLS Version LB-550. The optical bandgap was calculated from the transmittance data by using Tauc plot with a JASCO V-730 spectrophotometer. Immobilized PAni-TiO$_2$ nanoparticles were coated with gold using a Desk Sputter Coater (Dsr1 Nanostructural coating) and were seen by scanning electron microscope (SEM) and energy-dispersive X-ray spectroscopy (EDS) using TESCAN Vega 3.

Photocatalytic reactor

A photocatalytic reactor in pilot scale was designed and constructed for photocatalytic degradation of 1,2-DCE. Three cylindrical photocatalytic reactors (Fig. 4(A)) were connected to each other in series by Pneumatic tubes and mounted on the geometric center of three aluminum collectors (Fig. 4(B)). Collectors were used to reflect radiation of light back into the reactors. Collectors were 15 cm in diameter, with an axial distance of 20 cm from each other. Each reactor consists of three concentric cylinders

and a central lamp which enables the reactor to perform either visible or UV tests by replacing the lamp. Around the central lamp, a cylindrical quartz tube with an inner diameter of 2 cm for lamp protection, a cylindrical Pyrex tube with an inner diameter of 5.5 cm for making contact between pollutant, immobilized glass beads, dissolved oxygen, and irradiation of xenon lamp and another cylindrical Pyrex tube with an inner diameter of 10 cm for controlling the temperature of the reaction under 15 °C through the process were mounted, respectively. A 6-L wastewater tank (Fig. 4(C)) was made of Plexiglas and equipped with a 400-W heater, a temperature sensor, and a mechanical mixer. An 8-L water tank (Fig. 4(D)) was made of Plexiglas and equipped with a water pump, a temperature sensor, and a submersible pump. An 8-L temperature-adjusting tank (Fig. 4(E)) was made of Plexiglas and equipped with a submersible pump and a 400-W heater. The two submersible pumps were used for the circulation of water between the water tank and temperature-adjusting tank. Ice cubes were used for cooling down the water temperature. As shown in Fig. 4(F), a water flow meter was used to regulate the flow rate of wastewater between 6 and 60 L per h. In addition, an air flow meter (Fig. 4(G)) was used to regulate the aeration of inlet air into the wastewater tank between 2 and 10 L per min. An aeration pump (Fig. 4(H)) was used with a flow rate of 45 L/min (Hailea brand, ACO 308, 22 W). A water pump (Fig. 4(I)) was used with a flow rate of 10 L/min (victory/Hachaso's brand centrifuge pump, 90 W). A wastewater pump (Fig. 4(J)) was used with a flow rate of 10 L/min (victory/Hachaso's brand centrifuge pump, 120 W). The control panel of the photocatalytic reactor includes a power switch (Fig. 4(K)), 5 digital temperature controller
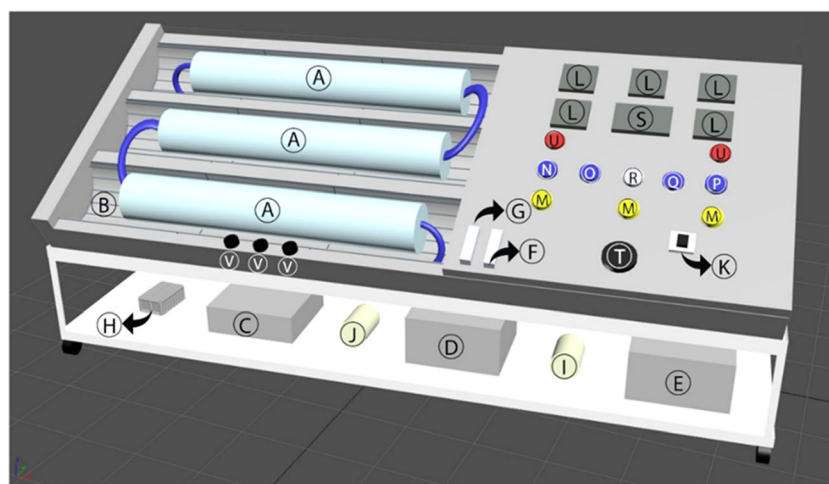

Fig. 4 Schematic of the photocatalytic reactor designed and constructed for photocatalytic degradation of 1,2-DCE. (A) Cylindrical photocatalytic reactors. (B) Aluminum collectors. (C) Wastewater tank. (D) Water tank. (E) Temperature adjusting tank. (F) Wastewater flow meter. (G) Air flow meter. (H) Aeration pump. (I) Water pump. (J) Wastewater pump. (K) Power switch. (L) Digital temperature controller display. (M) On/off switches for lamps. (N) Wastewater pump. (O) Water pump. (P) Mixer. (Q) Water circulation between submersible pumps. (R) Air pump. (S) Water level monitoring. (T) Controller for heater temperature. (U) On/off switch for heaters. (V) Sampling port for each reactor

displays (Fig. 4(L), Autonics brand model TCN4S), a water level monitoring controller (Fig. 4(S)), and a thermostatic temperature control valve (Fig. 4(T)). Other parts of the control panel are managed by on/off switches of lamps (Fig. 4(M)), wastewater pump (Fig. 4(N)), water pump (Fig. 4(O)), mixer (Fig. 4(P)), water circulation between submersible pumps (Fig. 4(Q)), air pump (Fig. 4(R)), heaters (Fig. 4(U)), and sampling ports (Fig. 4(V)).

Experimental design

In this research, the response surface method (RSM) based on the central composite design (CCD) was applied for designing experiments by using Design-Expert Software (Stat-Ease Design Expert v11.1.0.1, trial version). Independent parameters were initial 1,2-DCE concentration (A), residence time (B), pH (C), and coating mass (D). The removal efficiency of 1,2-DCE was considered the response parameter for 1,2-DCE degradation. Range and level of independent parameters were selected based on literature and preliminary experiments, as depicted in Table 1.

The total number of experiments was 27, including 16 factorial, 8 axial, and 3 central runs. The proposed RSM regression equation with multiple independent variables can be done in the following form:

$$Y_{pred} = \beta_0 + \sum_{i=1}^{k} \beta_i x_i + \sum_{i=1}^{k} \beta_{ii} x_i^2 + \sum_{i\langle j}^{k} \beta_{ij} x_i x_j \qquad (2)$$

where Y_{pred} is predicted value of the response parameter; β_0 is constant coefficient; β_i is the linear effect of parameter x_i; β_{ii} is the second order effect of parameter x_i; and β_{ij} is interaction linear effect of parameter x_i and x_j (Sakkas et al. 2010).

Photocatalytic degradation of 1,2-DCE

Photocatalytic degradation of 1,2-DCE was investigated in the designed and built recirculating batch photocatalytic reactor. Five liters of synthetic wastewater containing desired concentration of 1,2-DCE was prepared. HCl and NaOH (2 M) were used for pH adjustment. All experiments were performed in wastewater flow of 50 L/h, aeration flow of 2 L/min, and radiation of a 150-W xenon lamp. At specified sampling times, a sample was withdrawn for GC-MS analysis according to the analytical method. The 1,2-DCE removal was obtained using the following equation:

$$1,2-\text{dichloroethane removal\%} = \frac{C_0 - C_t}{C_0} \times 100 \qquad (3)$$

where $C_o(mg/l)$ is the initial concentration of 1,2-DCE at $t = 0$ and $C_t(mg/l)$ is the concentration of 1,2-DCE at t.

Results and discussion

Characterization

The scanning electron microscopy (SEM) analysis was used for observing the glass beads surface. The comparison of Fig. 5 a and b showed that PAni-TiO₂ nanoparticles were successfully immobilized on the surface of glass beads and particles were almost spherical and TiO₂ was uniformly distributed in the PAni matrix. Figure 5 c and d illustrate that SEM images of the cross section of coated glass beads. The coating layer thickness was about 2.74 μm. Results of SEM were in agreement with previous studies (Sabbaghi et al. 2015; Zhang et al. 2006). EDS spectra of uncoated and coated glass beads were depicted in Fig. 5 e and f, respectively. Based on the peaks of the Si, Ti, O, C, and N elements, the presence of TiO₂ and PAni (C_6H_7N) on the surface of glass beads was proved.

The crystal structures of the TiO₂, PAni, and PAni-TiO₂ nanocomposite were studied by the XRD measurement. As shown in Fig. 6, TiO₂ had 2θ peak values of 25.51°, 38.04°, 48.20°, 54.02°, 55.22°, 62.94°, and 75.30°. The results showed that with the addition of TiO₂, the crystallization of the PAni molecular chain was reduced. Results also showed that PAni deposition on the surface of TiO₂ did not affect the crystallinity of TiO₂ nanoparticles. Therefore, TiO₂ was found in the anatase form in the PAni-TiO2 nanocomposite. This is due to the fact that when the deposited PAni is absorbed on the surface of TiO₂ nanoparticles, the molecular chain of the absorbed PAni is tethered and the degree of crystallinity decreases (Sabbaghi et al. 2015; Zhang et al. 2006).

Figure 7 shows the FTIR spectrum for TiO₂, PAni, and the PAni-TiO₂ nanocomposite. As can be seen in the figure, the main characteristic peaks of the PAni-TiO₂ nanocomposite are as follows: the band at 2925.11 and 3433.84 cm⁻¹ may be assigned to hydrogen-bonded N–H and non-hydrogen bonded N–H stretching vibration between imine and amine sites (Sabbaghi et al. 2015; Zheng et al. 1997). The bands at 1563.99 and 1477.54 cm⁻¹ can be associated to C=C and C=N for the benzenoid and quinonoid units. The bands at 1295.97 and 1242.28 cm⁻¹ were assigned to the C–N for the benzenoid unit. The band at 801.08 cm⁻¹ was attributed to the C–C, and C–H for the benzenoid unit. The specific peaks of TiO₂ were at 1128.65 and 506.08 cm⁻¹. The peaks of PAni at 1295.97, 1477.54, and 1563.99 cm⁻¹ were associated with C–N and C=N bonds (Niu et al. 2003; Sabbaghi et al. 2015; Somani et al. 1999; Zhang et al. 2006). Based on the results, the composition of TiO₂ and PAni strengthened the hydrogen bonding of the PAni complex which resulted in a strong interaction between TiO₂ and PAni.

The particle size analysis (PSA) was used to achieve a better view of the synthesized PAni-TiO₂ dimensions. As shown in Fig. 8, the mean diameter of particles was 33.5

Table 1 Range and level of independent parameters

Factors	Units	$-\alpha$	Low (-1)	Middle (0)	High ($+1$)	$+\alpha$
A: 1,2 DCE concentration	mg/L	100	150	200	250	300
B: residence time	min	60	120	180	240	300
C: pH		3	5	7	9	11
D: coating mass	mg/cm^2	0.4	0.5	0.6	0.7	0.8

nm. Based on this result, it might be claimed that the synthesized PAni-TiO$_2$ particles were at nanoscale.

As shown in Fig. 9a, in the visible light range, the PAni-TiO$_2$ nanocomposite absorption was higher than the pure TiO$_2$, but in the UV range, pure TiO$_2$ absorption was higher than the PAni-TiO$_2$ nanocomposite. This finding is in agreement with previous researches (Sabbaghi et al. 2015; Yang et al. 2017). The optical bandgap of TiO$_2$ and PAni-TiO$_2$

Fig. 5 SEM images of **a** uncoated glass beads, **b** coated glass beads, **c** cross image of coated glass bead, and **d** cross image with coating thickness measurement. EDS spectra for **e** uncoated glass beads and **f** coated glass beads
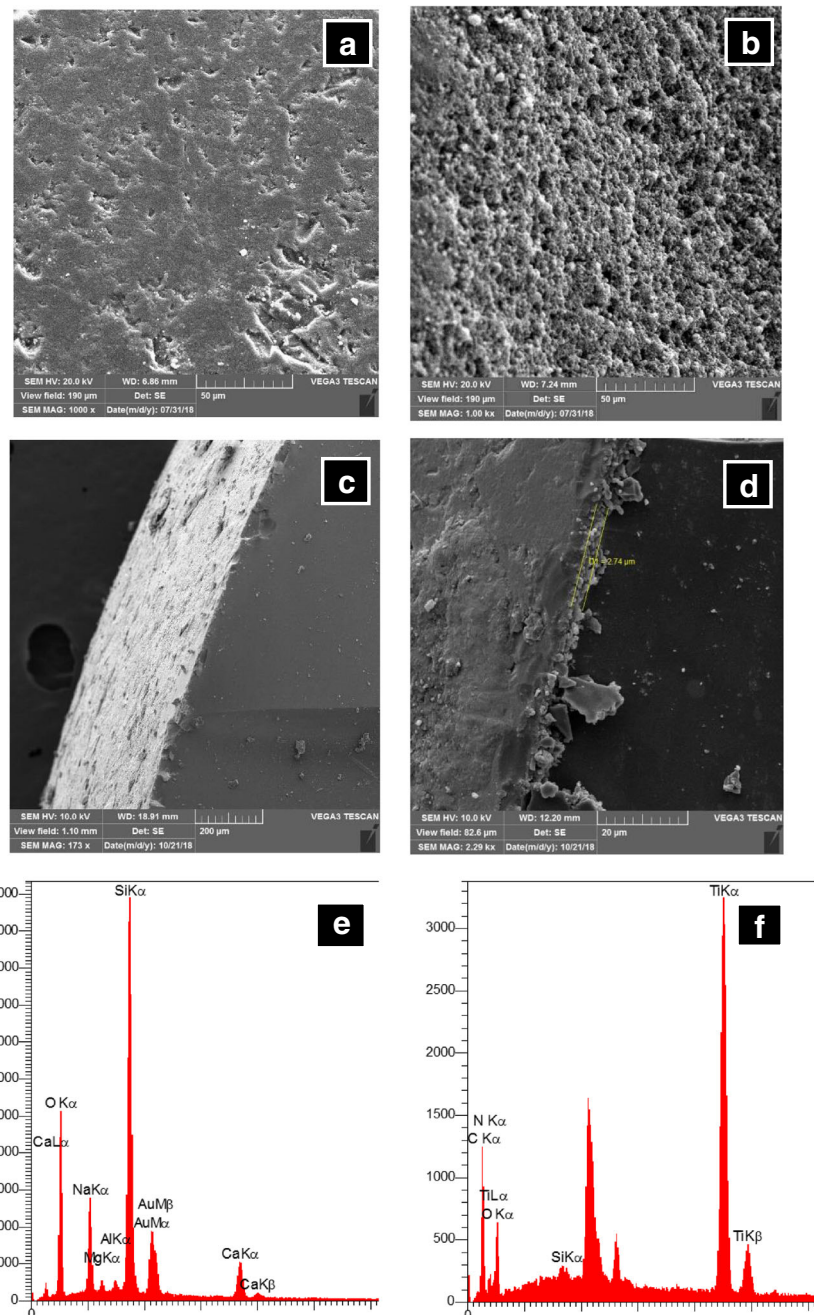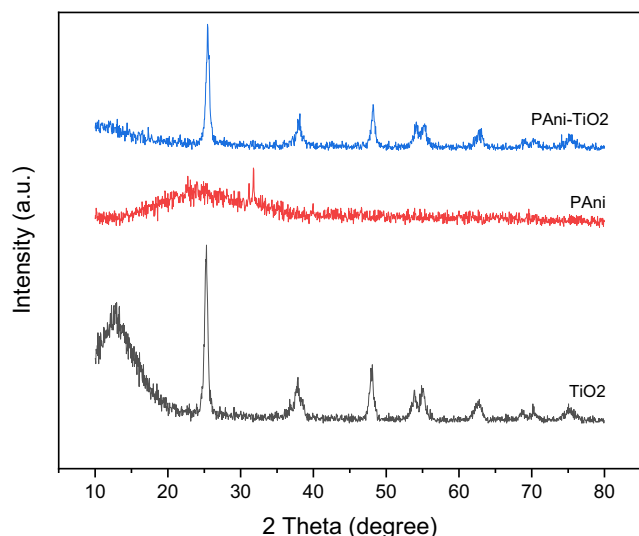
Fig. 6 XRD patterns of PAni, TiO$_2$, and PAni-TiO$_2$ nanocomposite

Fig. 8 PSA pattern of PAni-TiO$_2$ nanocomposite

TiO$_2$. Hence, PAni-TiO$_2$ nanocomposite showed better photo-catalytic activity under visible light irradiation.

RSM modeling

Designed experiments, actual removal percent, and RSM-predicted removal percent of the experiments are shown in Table 2.

Final RSM model equation in terms of actual factors is as follows:

was evaluated from the absorption spectrum using the Tauc relation (Mirbagheri and Sabbaghi 2018a; Soltani et al. 2014):

$$\alpha h v = B \left(h v - E_g \right)^n \tag{4}$$

where $\alpha = 2.303\ A/d$, A = absorbance and $d = 1$ for the standard quartz cell; $hv = hc/\lambda$, h is Planck's constant (6.6261×10^{-34} j.s.), c is the light velocity (3×10^8 m/s), and λ is the wavelength (nm); B is a constant; E_g is the average bandgap; and n is the type of transition. For $n = 0.5$, E_g is the direct allowed bandgap (Mohammadikish et al. 2013; Yang et al. 2017). As shown in Fig. 9b, the evaluated band gap of pure TiO$_2$ and PAni-TiO$_2$ nanocomposite was estimated from the linear portion of the $(\alpha h v)^2$ versus hv plots about 3.3 and 2.4 eV, respectively. This result indicated that the bandgap of PAni-TiO$_2$ nanocomposite was less than the bandgap of pure
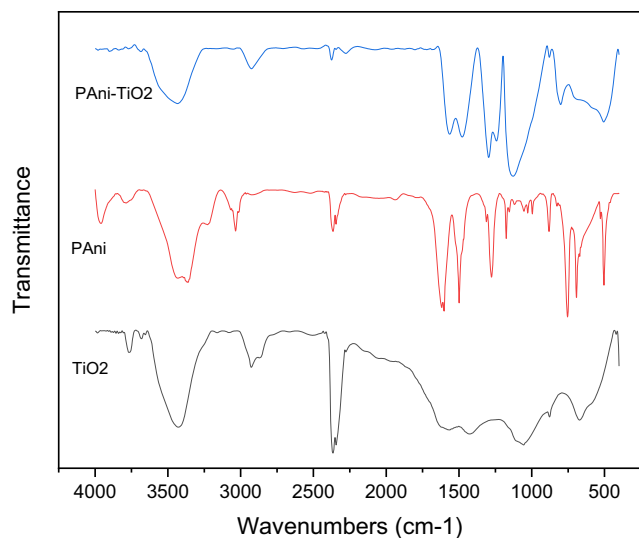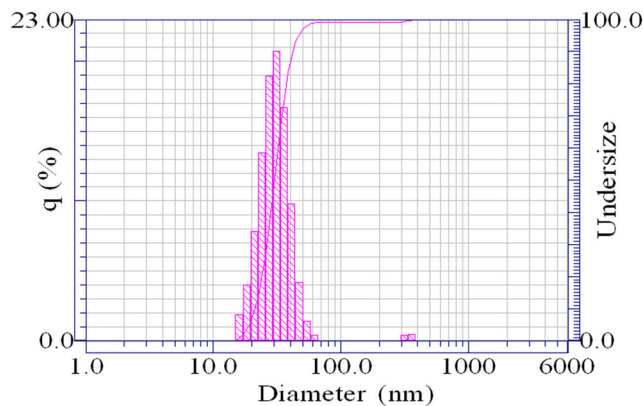
$$
\begin{aligned}
1,2-\text{DCE Removal} = \quad & + 7.37151 + 0.045054 \\
& \times 1,2\text{-DCE Concentration} \\
& + 0.550304 \\
& \times \text{Residence Time} - 0.156145 \\
& \times \text{pH} - 8.16469 \\
& \times \text{Coating Mass} - 0.000890 \\
& \times \text{Residence Time}^2 \tag{5}
\end{aligned}
$$

As shown in Table 3, the quadratic model was suggested due to the lack of fit test and model summary statistics. Afterward, the analysis of variance (ANOVA) was used for checking the model adequacy. According to the ANOVA table (Table 4), The F-value of 143.42 indicated that the model was significant. P values less than 0.05 indicate that model terms are significant. In this case, A, B, and B^2 were significant model terms. The lack of fit F-value of 0.51 implied that it could be neglected in comparison with the pure error. The predicted R^2 of 0.9870 and adjusted R^2 of 0.9718 were in reasonable agreement; i.e., the difference was not more than 0.2. Adeq precision measures the signal to noise ratio. A ratio greater than 4 is desirable. The ratio of 44.413 implied that the model could predict the experimental data with reasonable precision.
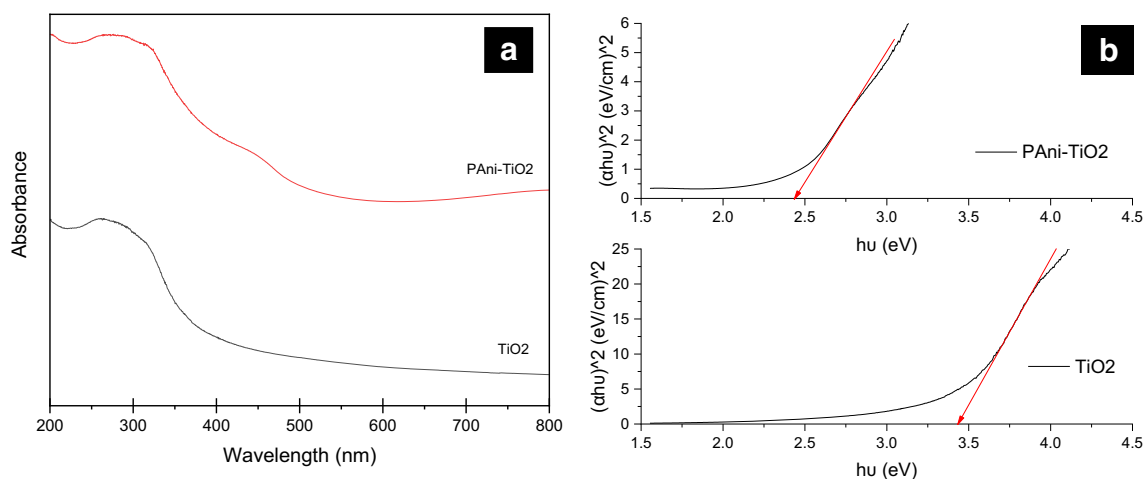

Fig. 7 FTIR spectra of PAni, TiO$_2$, and PAni-TiO$_2$ nanocomposite

Fig. 9 **a** UV-Vis absorption spectra and **b** Tauc plot of pure TiO_2 and PAni-TiO_2 nanocomposite

Figure 10a is a graph of the predicted response values versus the actual response values. The purpose of this figure is to check the accuracy of values predicted by the model. As illustrated, the proposed model could accurately predict the experimental data. The normal probability plot indicates whether the residuals follow a normal distribution, thus follow the straight line. As shown in Fig. 10b, the pattern was not like an S-shaped curve. Therefore, the studentized residuals followed a normal distribution.

Effect of operational parameters on the 1,2-DCE removal

Effect of operational parameters including 1,2-DCE concentration (A), residence time (B), pH (C), and coating mass (D) on the 1,2-DCE removal efficiency is shown in Fig. 11.

Effect of initial 1,2-DCE concentration

During the production of 1000 kg of 1,2-DCE, about 0.4 m^3 wastewater with 50–200 mg/L of 1,2-DCE is produced (Eydivand and Nikazar 2015). Therefore, in this study, initial 1,2-DCE concentration was selected in the range of 150–250 mg/L. As shown in Fig. 11a, in this range, the increase in the initial concentration of 1,2-DCE increased the photocatalytic degradation. This result was in agreement with the findings of previous studies (Eydivand and Nikazar 2015; Hung et al. 2008). This result showed that the used photocatalyst (packed bed–coated glass beads) had the ability for degradation of higher concentrations of 1,2-DCE. This is a great advantage for the industrialization of the reactor for photocatalytic degradation of 1,2-DCE.

The photocatalytic removal usually increases with increasing initial concentration of pollutant to a certain level.
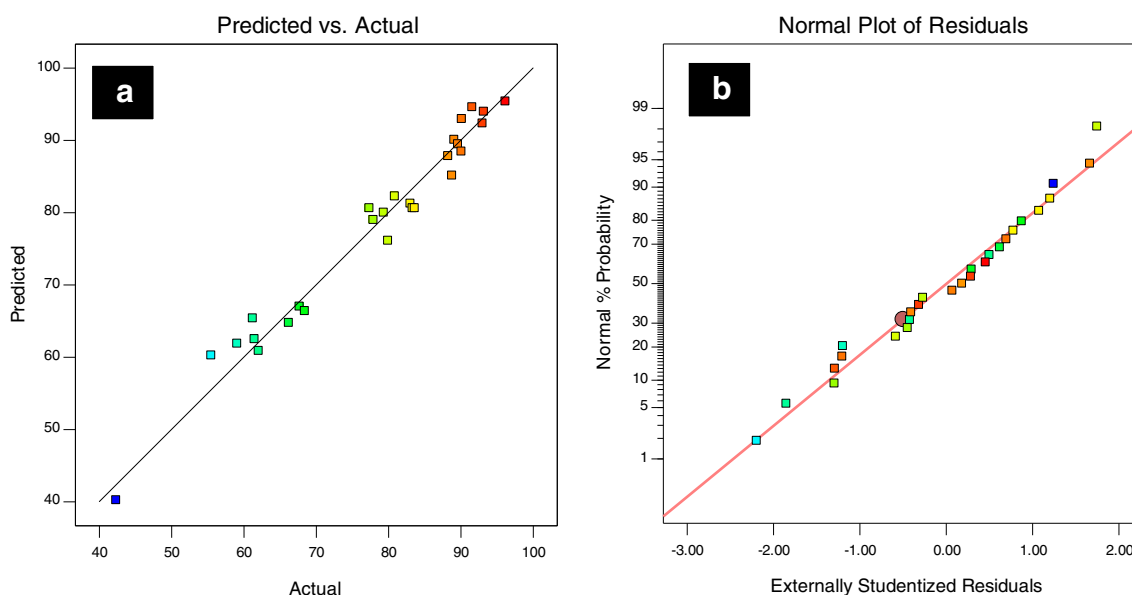

Fig. 10 **a** Actual values versus predicted values and **b** normal probability of studentized residuals

Table 2 CCD designed experiments, actual removal percent, and RSM-predicted removal values

Run	Space type	A: 1,2-DCE concentration (mg/L)	B: residence time (min)	C: pH	D: coating mass (mg/cm²)	Removal (actual) (%)	Removal (RSM-predicted) (%)
1	Axial	200	180	7	0.8	77.93	78.98
2	Factorial	150	240	5	0.7	90.10	88.44
3	Factorial	250	240	9	0.5	93.20	93.96
4	Factorial	150	240	5	0.5	89.10	90.08
5	Axial	200	60	7	0.6	42.34	40.20
6	Factorial	150	120	9	0.7	55.48	60.23
7	Center	200	180	7	0.6	83.33	80.61
8	Axial	300	180	7	0.6	88.80	85.11
9	Factorial	250	240	9	0.7	93.01	92.32
10	Axial	200	180	11	0.6	79.35	79.98
11	Axial	100	180	7	0.6	79.95	76.10
12	Center	200	180	7	0.6	83.64	80.61
13	Factorial	150	120	9	0.5	59.08	61.86
14	Factorial	250	120	9	0.5	68.43	66.37
15	Factorial	250	240	5	0.5	91.59	94.58
16	Axial	200	180	7	0.4	80.87	82.24
17	Factorial	250	120	5	0.7	61.24	65.36
18	Factorial	250	240	5	0.7	90.14	92.95
19	Factorial	250	120	5	0.5	67.70	66.99
20	Factorial	150	240	9	0.7	88.26	87.82
21	Axial	200	300	7	0.6	96.18	95.38
22	Center	200	180	7	0.6	77.36	80.61
23	Factorial	150	120	5	0.7	62.05	60.85
24	Axial	200	180	3	0.6	83.04	81.23
25	Factorial	150	240	9	0.5	89.62	89.45
26	Factorial	250	120	9	0.7	66.22	64.73
27	Factorial	150	120	5	0.5	61.48	62.49

Eventually, with a further increase in the initial concentration of the pollutant, the photocatalytic removal decreases. This decrease is probably due to the following reasons: (1) by increasing the initial concentration of the pollutant to a certain level, the pollutant molecules can occupy all active sites of the photocatalyst. Further increase in the initial concentration of the pollutant increases the need for reactive species (OH• and O_2•−) for photocatalytic degradation of the pollutant.

Table 3 Lack of fit test and model summary statistics

Lack of fit test						
Source	Sum of squares	df	Mean square	F-value	p value	
Linear	394.58	20	19.73	1.58	0.4596	
2FI	343.50	14	24.54	1.96	0.3890	
Quadratic	41.67	10	4.17	0.3328	0.9049	Suggested
Cubic	20.49	2	10.24	0.8180	0.5501	Aliased
Pure error	25.04	2	12.52			
Model summary statistics						
Source	Std. Dev.	R^2	Adjusted R^2	Predicted R^2	PRESS	
Linear	4.37	0.9181	0.9032	0.8773	628.94	
2FI	4.80	0.9281	0.8832	0.8631	701.48	
Quadratic	2.36	0.9870	0.9718	0.9422	296.36	Suggested
Cubic	3.37	0.9911	0.9423	0.4135	3006.20	Aliased

Table 4 ANOVA test for response surface quadratic model

Source	Sum of squares	df	Mean square	*F*-value	*p* value	
Model	4979.69	5	995.94	143.42	< 0.0001	Significant
A—1,2-DCE concentration	121.79	1	121.79	17.54	0.0004	
B—residence time	4565.77	1	4565.77	657.50	< 0.0001	
C—pH	2.34	1	2.34	0.3371	0.5677	
D—coating mass	16.00	1	16.00	2.30	0.1440	
B^2	273.79	1	273.79	39.43	< 0.0001	
Residual	145.83	21	6.94			
Lack of fit	120.78	19	6.36	0.5077	0.8330	Not significant
Pure error	25.04	2	12.52			
Cor total	5125.52	26				
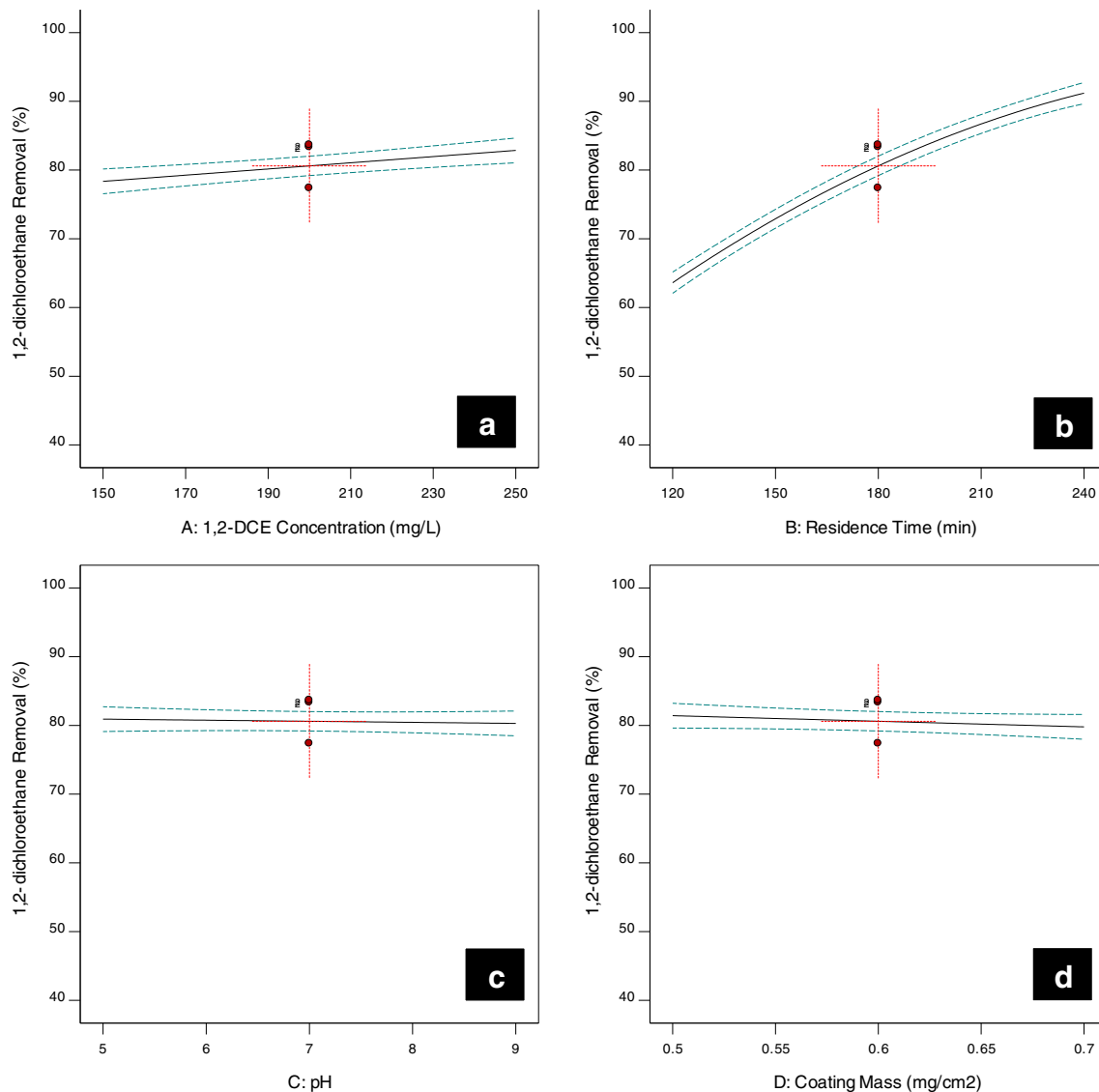
Fig. 11 Effects of operational parameters on the 1,2-DCE removal efficiency: effect of **a** initial 1,2-DCE concentration, **b** residence time, **c** pH, **d** coating mass
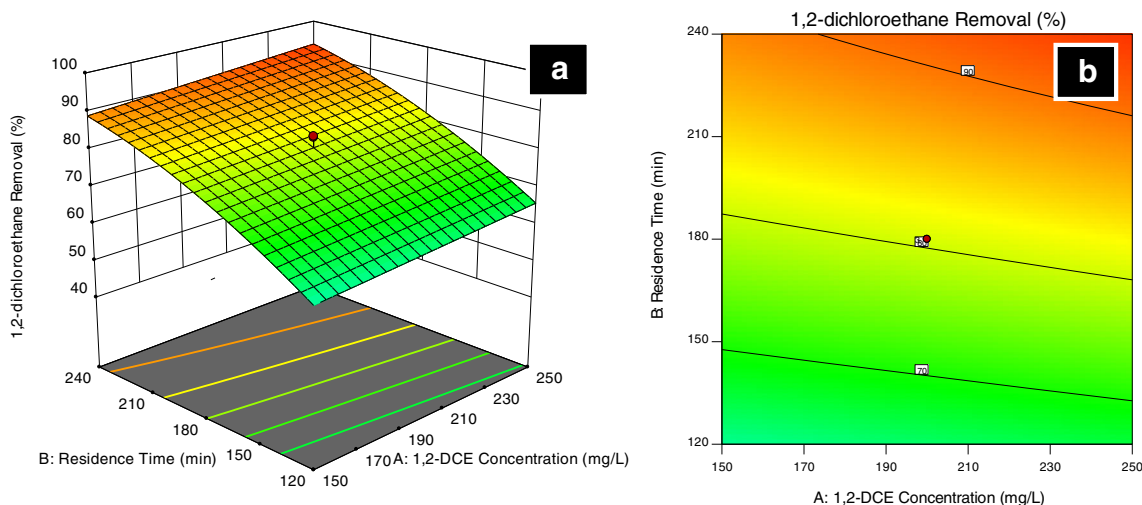
Fig. 12 Images of **a** 3D response surface graph and **b** contour plot for 1,2-DCE degradation

However, the formation of reactive species on the surface of the photocatalyst remains constant for a constant amount of photocatalyst, irradiation time, and irradiation intensity. Therefore, the pollutant degradation rate is decreased. (2) Increasing the initial concentration of the pollutant can lead to the production of intermediate products that can be adsorbed onto the photocatalyst active sites and compete with pollutant molecules, which may result in the inactivation of the photocatalyst active sites (Fathinia et al. 2010). (3) Increasing the initial concentration of the pollutant can decrease the number of absorbed photons on the surface of the photocatalyst which indicates a decrease in the production of reactive species of OH• and O_2•– (Konstantinou and Albanis 2004).

Effect of residence time

Photocatalytic degradation reactions can be initiated by irradiation of a photon with sufficient energy on the photocatalyst surface (Daneshvar et al. 2003, 2004; Habibi et al. 2005). Therefore, It is obvious that photocatalytic degradation increases with increasing irradiation time. In this study, residence time was selected in the range of 120–240 min. As shown in Fig. 11b, the photocatalytic degradation of 1,2-DCE was about 60%, 90%, and 95% after 120 min, 240 min, and 300 min, respectively. Rate of photocatalytic

degradation decreased after 240 min because the pollutant molecules cannot occupy all active sites of the photocatalyst in low pollutant concentrations (Nikazar et al. 2008; Sabbaghi and Doraghi 2016). Complete degradation was achieved after 360 min.
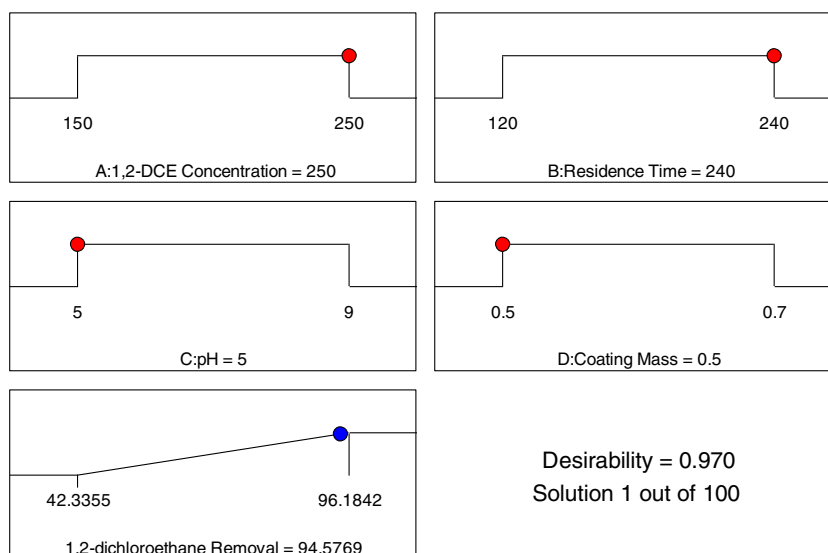
Effect of pH

In the present study, the effect of pH on photocatalytic degradation of 1,2-DCE in the range of 5 to 9 was investigated. As illustrated in Fig. 11c, results showed that the photocatalytic degradation remains at about 80% in the range of pH from 5 to 9. A similar effect of pH on photocatalytic degradation of 1,2-DCE was reported previously where the initial pH of 3, 7, and 10 was selected for photocatalytic degradation experiments. Based on the results, the initial pH had no significant effect on the photocatalytic degradation of 1,2-DCE (Eydivand and Nikazar 2015). The high removal efficiency in a wide range of pH is a great advantage for the industrialization of the photocatalytic degradation of 1,2-DCE because the results indicated that there is no need for pH adjustment.

Generally, the PH effect on the photocatalytic degradation is complicated due to its multiple roles, and the observed effect depending on the type of pollutant and the point of zero charge (PZC) of the photocatalyst. The PZC is the point at which the photocatalyst surface charge is zero. Below the

Table 5 Results of numerical optimization

Name	Goal	Lower limit	Upper limit	Lower weight	Upper weight	Importance
A: 1,2-DCE concentration	Is in range	150	250	1	1	3
B: residence time	Is in range	120	240	1	1	3
C: pH	Is in range	5	9	1	1	3
D: coating mass	Is in range	0.5	0.7	1	1	3
1,2-DCE removal	Maximize	42.3355	96.1842	1	1	5

Fig. 13 Desirability ramp for numerical optimization

A:1,2-DCE Concentration = 250 (150 – 250)

B:Residence Time = 240 (120 – 240)

C:pH = 5 (5 – 9)

D:Coating Mass = 0.5 (0.5 – 0.7)

1,2-dichloroethane Removal = 94.5769 (42.3355 – 96.1842)

Desirability = 0.970
Solution 1 out of 100

PZC, the surface charge of the photocatalyst becomes positive and absorbs the anionic compounds. Above the PZC, the surface charge of the photocatalyst becomes negative and repels the anionic compounds (Bechambi et al. 2015; Eydivand and Nikazar 2015). The holes are considered as the main factors of photocatalytic degradation at low pH and hydroxyl radicals are considered as the main factors of photocatalytic degradation at neutral or high pH (Akpan and Hameed 2009; Eydivand and Nikazar 2015).

Effect of coating mass

Results of the previous study showed that when the coating mass was increased in the range of 0.1–0.5 mg/cm^2, a slight increase in photocatalytic degradation was observed (Mohsenzadeh et al. 2019a). Therefore, in this study, the effect of coating mass in the range of 0.5–0.7 mg/cm^2 on the photocatalytic degradation of 1,2-DCE was investigated. The results showed that the increase in coating mass did not significantly affect photocatalytic degradation. According to Fig. 11d, there even was a slight decrease in photocatalytic degradation. The maximum photocatalytic degradation efficiency occurred when the coating mass was about 0.5 mg/cm^2. Generally, when the coating layer is thin, the absorption of

light is not enough, so the photocatalyst layer is not highly active. When the coating layer is increased, the light-induced electron-hole pairs are created, which maximizes the photocatalytic degradation. A further increase in the coating layer increases the recombination rate and decreases the photocatalytic degradation of 1,2-DCE.

Many previous studies have shown that there is an optimum thickness for the coating mass (Chen et al. 2000, 2001; Choi et al. 2001; Yu et al. 2003). Chen et al. reported that photocatalytic degradation increased with increasing of the coating mass to an optimum value. A further increase in the coating mass did not affect the photocatalytic degradation (Chen et al. 2000). Choi et al. reported that the optimum thickness of TiO$_2$ coating layer was in the range of 1–2 μm, and a further increase in the thickness of the coating layer decreased the photocatalytic degradation efficiency (Choi et al. 2001). Bouarioua and Zerdaoui proved that increasing weight of coating mass with increasing number of layers to a certain level resulted in good adhesion with stable form of the immobilized photocatalyst. However, the over increasing thickness of TiO$_2$ films led to decreasing the electrostatic attraction between the two surfaces of TiO$_2$ particles and the support, hence a weakness of the adhesion between them (Bouarioua and Zerdaoui 2017).

Table 6 Confirmation test and results

Optimized test									
1,2-DCE concentration			Residence time		pH		Coating mass		
250			240		5		0.5		
Result									
Solution 1 of 100 response	Predicted mean	Predicted median	Observed	Std. Dev.	n	SE Pred	95% PI low	Data mean	95% PI high
1,2-DCE removal	93.533	93.533		2.63518	3	2.85326	87.5994	88.84	99.4667

Fig. 14 Kinetics of photocatalytic degradation of 1,2-DCE in optimized conditions

Time	C_t	Removal	$\ln(C_0/C)$
min	mg/l	%	
60	159.858689	36.05652	0.447171
120	102.727284	58.90909	0.889383
180	56.8859505	77.24562	1.480413
240	27.8853811	88.84585	2.193358
300	10.2223394	95.91106	3.196885
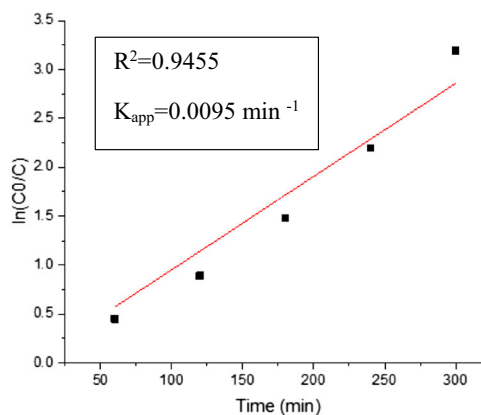
Figure 12a shows a 3D response surface and Fig. 12b illustrates contour plot of 1,2-DCE photocatalytic degradation as a function of 1,2-DCE initial concentration and residence time. Three-dimensional response surface was obtained from Eq. 5 using experimental data. Based on this figure, it was observed that with increasing 1,2-DCE concentration and residence time, photocatalytic degradation smoothly increased. As a result, the designed and built photocatalytic reactor can be used for degradation of higher initial 1,2-DCE concentrations. Therefore, there is no need to dilute the 1,2-DCE wastewater in the industrialized scale photocatalytic reactor.

Optimization and confirmation

According to Table 5, numerical optimization was performed by design expert software to find a specific point of the response surface that maximizes the desirability function. The results are depicted in Fig. 13. The software optimized 1,2-DCE removal (94.58%) by optimizing independent variables of 1,2-DCE concentration, residence time, pH, and coating mass at 250 mg/L, 240 min, 5, and 0.5 mg/cm², respectively.

The validation tests were performed in optimized conditions to evaluate the model's accuracy to predict the optimal values of the independent variables. Table 6 reveals the average photocatalytic degradation of the optimized tests was 88.84%, which fell within 95% of the prediction interval bands, which confirmed that the optimization by RSM technique was successful.

Two-sided confidence = 95%

Kinetics study

To study the kinetics of photocatalytic degradation of 1,2-DCE, photocatalytic degradation experiments were performed under optimal conditions of 1,2-DCE concentration of 250 mg/L, pH of 5, and coating mass of 0.5 mg/cm². The kinetic of the heterogeneous photocatalytic degradation process follows the Langmuir-Hinshelwood model (Martínez et al. 2011; Mirbagheri and Sabbaghi 2018b). Usually, first-order kinetics

seems to be adequate, and various studies were well fitted by the pseudo-first-order model. The pseudo-first-order model can be expressed as follows (Konstantinou and Albanis 2004; Nguyen-Phan et al. 2011):

$$\ln \frac{C}{C_0} = -K_{app}t \qquad (6)$$

where C is the pollutant concentration at time t, C_0 is the pollutant initial concentration, K_{app} is the value of the apparent first-order rate constant, and t is the time. According to Fig. 14, the pseudo-first kinetics model was tested with the experimental data of the optimized tests and the results indicated that the first-order rate constant was 0.0095 min^{-1} with R^2 of 0.9455.

Conclusion

In this study, synthesis of PAni-TiO2 was confirmed by morphology tests. Immobilization of the photocatalyst on the surface of glass beads was successfully achieved by a modified dip coating and heat attachment method. A new pilot scale packed bed photocatalytic reactor was designed and constructed. Based on the results, 1,2-DCE was completely degraded using immobilized PAni-TiO$_2$ nanocomposite under visible light irradiation. PAni-TiO$_2$ nanocomposite enhanced the photocatalytic degradation of 1,2-DCE under visible light irradiation by reducing bandgap and hindering recombination. Photocatalytic degradation of 1,2-DCE was modeled and optimized by RSM technique. The optimum conditions for 1,2-DCE photocatalytic degradation were the 1,2-DCE initial concentration of 250 mg/L, the residence time of 240 min, pH of 5, and coating mass of 0.5 mg/cm², which resulted in 88.84% photocatalytic degradation. Kinetic of the photocatalytic degradation process was studied under optimum conditions. It was found that there was no need for 1,2-DCE wastewater dilution and pH adjustment for achieving high degradation efficiency. These are great advantages for the industrialization of photocatalytic degradation of 1,2-DCE. To sum up, it seems

that the designed and constructed photocatalytic reactor has the potential for scaling up.

References

Akpan UG, Hameed BH (2009) Parameters affecting the photocatalytic degradation of dyes using TiO2-based photocatalysts: a review. J Hazard Mater 170:520–529

Antonopoulou M, Chondrodimou I, Bairamis F, Giannakas A, Konstantinou I (2017) Photocatalytic reduction of Cr (VI) by char/TiO$_2$ composite photocatalyst: optimization and modeling using the response surface methodology (RSM). Environ Sci Pollut Res 24: 1063-1072, Photocatalytic reduction of Cr(VI) by char/TiO2 composite photocatalyst: optimization and modeling using the response surface methodology (RSM)

APHA (2012) Standard methods for the examination of water and wastewater. APHA-AWWA-WEF, Washington, D.C.

Balasubramanian G, Dionysiou D, Suidan M, Subramanian V, Baudin I, Laîné J-M (2003) Titania powder modified sol-gel process for photocatalytic applications. J Mater Sci 38:823–831

Bechambi O, Sayadi S, Najjar W (2015) Photocatalytic degradation of bisphenol A in the presence of C-doped ZnO: effect of operational parameters and photodegradation mechanism. J Ind Eng Chem 32: 201–210

Bejankiwar R, Lalman JA, Seth R, Biswas N (2005) Electrochemical degradation of 1,2-dichloroethane (DCA) in a synthetic groundwater medium using stainless-steel electrodes. Water Res 39:4715–4724

Bijhanmanesh MJ, Etesami N (2016) Continuous dosing of fast initiator during vinyl chloride suspension polymerization: polymerization rate and PVC properties. J Appl Polym Sci 133:1–13

Bouarioua A, Zerdaoui M (2017) Photocatalytic activities of TiO2 layers immobilized on glass substrates by dip-coating technique toward the decolorization of methyl orange as a model organic pollutant. J Environ Chem Eng 5:1565–1574

Chen D, Li F, Ray AK (2000) Effect of mass transfer and catalyst layer thickness on photocatalytic reaction. AICHE J 46:1034–1045

Chen D, Li F, Ray AK (2001) External and internal mass transfer effect on photocatalytic degradation. Catal Today 66:475–485

Choi W, Ko JY, Park H, Chung JS (2001) Investigation on TiO2-coated optical fibers for gas-phase photocatalytic oxidation of acetone. Appl Catal B Environ 31:209–220

Daneshvar N, Salari D, Khataee A (2003) Photocatalytic degradation of azo dye acid red 14 in water: investigation of the effect of operational parameters. J Photoch Photobiol A 157:111–116

Daneshvar N, Salari D, Khataee A (2004) Photocatalytic degradation of azo dye acid red 14 in water on ZnO as an alternative catalyst to TiO2. J Photochem Photobiol A 162:317–322

De Wildeman S, Nollet H, Van Langenhove H, Verstraete W (2001) Reductive biodegradation of 1,2-dichloroethane by methanogenic granular sludge in lab-scale UASB reactors. Adv Environ Res 6: 17–27

Eydivand S, Nikazar M (2015) Degradation of 1,2-dichloroethane in simulated wastewater solution: a comprehensive study by photocatalysis using TiO2 and ZnO nanoparticles. Chem Eng Commun 202:102–111

Fathinia M, Khataee A, Zarei M, Aber S (2010) Comparative photocatalytic degradation of two dyes on immobilized TiO2 nanoparticles: effect of dye molecular structure and response surface approach. J Mol Catal A Chem 333:73–84

Habibi MH, Hassanzadeh A, Mahdavi S (2005) The effect of operational parameters on the photocatalytic degradation of three textile azo dyes in aqueous TiO2 suspensions. J Photoch Photobiol A 172: 89–96

Hajian M, Mirbagheri SA, Taqizade I, Javid AH (2017) Evaluation of chemical, biological and ecotoxicological characteristics of cresol and its Fenton's degradation products. Desalin Water Treat 82: 355–361

Huang B, Lei C, Wei C, Zeng G (2014) Chlorinated volatile organic compounds (Cl-VOCs) in environment—sources, potential human health impacts, and current remediation technologies. Environ Int 71:118–138

Hung W-C, Chen Y-C, Chu H, Tseng T-K (2008) Synthesis and characterization of TiO2 and Fe/TiO2 nanoparticles and their performance for photocatalytic degradation of 1,2-dichloroethane. Appl Surf Sci 255:2205–2213

Hung C-H, Yuan C, Li H-W (2017) Photodegradation of diethyl phthalate with PANi/CNT/TiO2 immobilized on glass plate irradiated with visible light and simulated sunlight—effect of synthesized method and pH. J Hazard Mater 322:243–253

Jinzhang G, Shengying L, Wu Y, Guohu Z, Lili B, Li S (2007) Preparation and photocatalytic activity of PANI/TiO2 composite film. Rare Metals 26:1–7

Khalilian H, Behpour M, Atouf V, Hosseini SN (2015) Immobilization of S, N-codoped TiO2 nanoparticles on glass beads for photocatalytic degradation of methyl orange by fixed bed photoreactor under visible and sunlight irradiation. Sol Energy 112:239–245

Khataee A (2009) Photocatalytic removal of CI Basic Red 46 on immobilized TiO2 nanoparticles: artificial neural network modelling. Environ Technol 30:1155–1168

Konstantinou IK, Albanis TA (2004) TiO2-assisted photocatalytic degradation of azo dyes in aqueous solution: kinetic and mechanistic investigations: a review. Appl Catal B Environ 49:1–14

Lin Y, Li D, Hu J, Xiao G, Wang J, Li W, Fu X (2012) Highly efficient photocatalytic degradation of organic pollutants by PANI-modified TiO2 composite. J Phys Chem C 116:5764–5772

Lin Y-H, Chou S-H, Chu H (2014) A kinetic study for the degradation of 1,2-dichloroethane by S-doped TiO$_2$ under visible light. J Nanopart Res 16:2539

Liu X, Vellanki BP, Batchelor B, Abdel-Wahab A (2014) Degradation of 1,2-dichloroethane with advanced reduction processes (ARPs): Effects of process variables and mechanisms. Chem Eng J 237: 300–307

Maleki SA, Mirzaei M, Azimi A (2016) COD reduction by TiO2/graphene photocatalytic treatment of ethylene dichloride in wastewater. Desalin Water Treat 57:13207–13212

Martínez C, Fernández M, Santaballa J, Faria J (2011) Kinetics and mechanism of aqueous degradation of carbamazepine by heterogeneous photocatalysis using nanocrystalline TiO2, ZnO and multiwalled carbon nanotubes–anatase composites. Appl Catal B Environ 102:563–571

Mirbagheri NS, Sabbaghi S (2018a) A Ti-doped γ-Fe 2 O 3/SDS nanophotocatalyst as an efficient adsorbent for removal of methylene blue from aqueous solutions. J Environ Manag 213:56–65

Mirbagheri NS, Sabbaghi S (2018b) A natural kaolin/γ-Fe2O3 composite as an efficient nano-adsorbent for removal of phenol from aqueous solutions. Microporous Mesoporous Mater 259:134–141

Mohammadi M, Sabbaghi S (2014) Photo-catalytic degradation of 2, 4-DCP wastewater using MWCNT/TiO2 nano-composite activated by UV and solar light. Environ Nanotech Monit Manage 1:24–29

Mohammadikish M, Davar F, Loghman-Estarki MR, Hamidi Z (2013) Synthesis and characterization of hierarchical ZnS architectures

based nanoparticles in the presence of thioglycolic acid. Ceram Int 39:3173–3181

Mohsenzadeh M, Mirbagheri SA, Sabbaghi S (2019a) Photocatalytic degradation of 1,2-dichloroethane using immobilized PAni-TiO2 nanocomposite in a pilot-scale packed bed reactor. Desalin Water Treat 155:72–83

Mohsenzadeh M, Mirbagheri SA, Sabbaghi S (2019b) Immobilized PAni-TiO2 nano-photocatalyst modeling for photocatalytic degradation of 1,2-dichloroethane using response surface methodology (RSM) and artificial neural network (ANN). Int J Mech Prod Eng Res Dev 9:731–744

Nam S-N, Cho H, Han J, Her N, Yoon J (2018) Photocatalytic degradation of acesulfame K: optimization using the Box–Behnken design (BBD). Process Saf Environ 113:10–21

Nekouei F, Nekouei S (2017) Comparative study of photocatalytic activities of Zn5 (OH) 8Cl2·H2O and ZnO nanostructures in ciprofloxacin degradation: response surface methodology and kinetic studies. Sci Total Environ 601: 508-517

Nguyen-Phan T-D, Pham VH, Shin EW, Pham H-D, Kim S, Chung JS, Kim EJ, Hur SH (2011) The role of graphene oxide content on the adsorption-enhanced photocatalysis of titanium dioxide/graphene oxide composites. Chem Eng J 170:226–232

Nikazar M, Gholivand K, Mahanpoor K (2008) Photocatalytic degradation of azo dye Acid Red 114 in water with TiO2 supported on clinoptilolite as a catalyst. Desalination 219:293–300

Niu Z, Yang Z, Hu Z, Lu Y, Han CC (2003) Polyaniline–silica composite conductive capsules and hollow spheres. Adv Funct Mater 13:949–954

Pham H, Boon N, Marzorati M, Verstraete W (2009) Enhanced removal of 1,2-dichloroethane by anodophilic microbial consortia. Water Res 43:2936–2946

Radoičić M, Ćirić-Marjanović G, Spasojević V, Ahrenkiel P, Mitrić M, Novaković T, Šaponjić Z (2017) Superior photocatalytic properties of carbonized PANI/TiO2 nanocomposites. Appl Catal B Environ 213:155–166

Sabbaghi S, Doraghi F (2016) Photo-catalytic degradation of methylene blue by ZnO/SnO2 nanocomposite. J Water Environ Nanotechnol 1: 27–34

Sabbaghi S, Mohammadi M, Ebadi H (2015) Photocatalytic degradation of benzene wastewater using PANI-TiO 2 nanocomposite under UV and solar light radiation. J Environ Eng 142:05015003

Sakkas VA, Islam MA, Stalikas C, Albanis TA (2010) Photocatalytic degradation using design of experiments: a review and example of the Congo red degradation. J Hazard Mater 175:33–44

Sakthivel S, Shankar M, Palanichamy M, Arabindoo B, Murugesan V (2002) Photocatalytic decomposition of leather dye: comparative study of TiO2 supported on alumina and glass beads. J Photoch Photobiol A 148:153–159

Salem MA, Al-Ghonemiy AF, Zaki AB (2009) Photocatalytic degradation of Allura red and Quinoline yellow with Polyaniline/TiO2 nanocomposite. Appl Catal B Environ 91:59–66

Salma A, Thoröe-Boveleth S, Schmidt TC, Tuerk J (2016) Dependence of transformation product formation on pH during photolytic and photocatalytic degradation of ciprofloxacin. J Hazard Mater 313: 49–59

Schnitzler DC, Zarbin AJ (2004) Organic/inorganic hybrid materials formed from TiO2 nanoparticles and polyaniline. J Braz Chem Soc 15:378–384

Soltani N, Saion E, Yunus WMM, Erfani M, Navasery M, Bahmanrokh G, Rezaee K (2014) Enhancement of visible light photocatalytic activity of ZnS and CdS nanoparticles based on organic and inorganic coating. Appl Surf Sci 290:440–447

Somani PR, Marimuthu R, Mulik U, Sainkar S, Amalnerkar D (1999) High piezoresistivity and its origin in conducting polyaniline/TiO2 composites. Synth Met 106:45–52

Tian M, Jian Y, Ma M, He C, Chen C, Liu C, Shi J-W (2019) Rational design of CrOx/LaSrMnCoO6 composite catalysts with superior chlorine tolerance and stability for 1,2-dichloroethane deep destruction. Appl Catal A Gen 570:62–72

Vazirzadeh M, Karbalaei-Heidari H, Mohsenzadeh M (2012) Bioethanol production from white onion by yeast in repeated batch. Iran J Sci Technol A 36:477–480

Wang S, Chen S, Lin Y, Kuo Y, Chen J, Kao C (2016) Acidification and sulfide formation control during reductive dechlorination of 1,2-dichloroethane in groundwater: Effectiveness and mechanistic study. Chemosphere 160:216–229

Wang T, Xu D, Fan Q, Rong W, Zheng J, Gao C, Li G, Zeng N, Guo T, Zeng L (2017) 1,2-Dichloroethane impairs glucose and lipid homeostasis in the livers of NIH Swiss mice. Toxicology 380:38–49

Yang C, Dong W, Cui G, Zhao Y, Shi X, Xia X, Tang B, Wang W (2017) Enhanced photocatalytic activity of PANI/TiO2 due to their photosensitization-synergetic effect. Electrochim Acta 247:486–495

Yu JC, Ho W, Lin J, Yip H, Wong PK (2003) Photocatalytic activity, antibacterial effect, and photoinduced hydrophilicity of TiO2 films coated on a stainless steel substrate. Environ Sci Technol 37:2296–2301

Zhang L, Liu P, Su Z (2006) Preparation of PANI–TiO2 nanocomposites and their solid-phase photocatalytic degradation. Polym Degrad Stab 91:2213–2219

Zheng W, Angelopoulos M, Epstein AJ, MacDiarmid A (1997) Experimental evidence for hydrogen bonding in polyaniline: mechanism of aggregate formation and dependency on oxidation state. Macromolecules 30:2953–2955